ISSN: 2083-389X
eISSN: 2084-3127

© J Hear Sci, 2022; 12(2): 9–19
DOI: 10.17430/JHS.2022.12.2.1

FROM HAIR BUNDLE TO EARDRUM: AN EXTENDED MODEL FOR THE GENERATION OF SPONTANEOUS OTOACOUSTIC EMISSIONS BY THE LIZARD EAR

Hero P. Wit[1AC-F], Andrew Bell[2D-F]

[1] Department of Otolaryngology/Head and Neck Surgery, Medical Center, University of Groningen, Graduate School of Medical Sciences, Groningen, Netherlanads
[2] Eccles Institute of Neuroscience, John Curtin School of Medical Research, The Australian National University, Canberra, Australia

Corresponding author: Hero P. Wit, Otolaryngology/Head and Neck Surgery, University of Groningen, Hanzeplein 1, 9713GZ, Groningen, Netherlands; email: hero.wit@ziggo.nl

Contributions:
A Study design/planning
B Data collection/entry
C Data analysis/statistics
D Data interpretation
E Preparation of manuscript
F Literature analysis/search
G Funds collection

Abstract

Background: An earlier oscillator model for the generation of spontaneous otoacoustic emissions (SOAEs) from the lizard ear is extended with a connection of the oscillators to the basilar papilla, to make it possible that these SOAEs can be transported to the tympanic membrane, to be emitted.

Material and methods: The generators of spontaneous otoacoustic emissions are modelled as a one-dimensional array of Hopf-resonators. The resonators (or oscillators) are coupled to their neighbours, and to the basilar papilla. The papilla is modelled as a rigid structure, that is flexibly connected to its surroundings.

Results: Frequency spectra are given for different sets of coupling parameters, both for nearest neighbour coupling of the oscillators, and for coupling to the papilla, and also after the introduction of irregularities in the damping of the oscillators. Waterfall and density plots show clustering of the oscillators in frequency plateaus, and entrainment of a cluster of oscillators by an externally applied sinusoidal force. All these model outcomes correspond with characteristics of SOAEs emitted by real lizard ears.

Conclusions: The present model is a useful extension of an earlier model. Because its characteristics differ from that of a model that is used to describe the generation of SOAEs by mammalian ears, it revives the discussion whether different models are needed for SOAE generation in different animal species

Key words: inner ear • coupled oscillators • basilar papilla • travelling waves • self-sustaining • frequency plateaus

OD PĘCZKA KOMÓREK SŁUCHOWYCH DO BŁONY BĘBENKOWEJ: ROZSZERZONY MODEL GENERACJI SPONTANICZNYCH EMISJI OTOAKUSTYCZNYCH W UCHU JASZCZUREK

Streszczenie

Wprowadzenie: Wcześniejszy model oscylatora generacji spontanicznych emisji otoakustycznych (SOAE) w uchu jaszczurki został rozszerzony o połączenie z oscylatorami brodawki podstawnej celem umożliwienia przeniesienia tych SOAE na błonę bębenkową, gdzie są emitowane.

Materiał i metody: Generatory spontanicznych otoemisji akustycznych są modelowane jako jednowymiarowy zestaw rezonatorów Hopfa, które są sparowane ze swoimi sąsiadami i z brodawką podstawną. Brodawka podstawna jest modelowana jako struktura sztywna elastycznie połączona ze swoim otoczeniem.

Wyniki: Zakresom częstotliwości przypisano różne zestawy parametrów sprzężenia: dla najbliższego sprzężenia oscylatorów, dla sprzężenia z błoną podstawną oraz po wprowadzeniu nieregularności w tłumieniu oscylatorów. Wykresy kaskadowe i gęstości pokazują zarówno skupiska oscylatorów w płaskiej części wykresu częstotliwości, jak i wciąganie skupisk oscylatorów przez siłę sinusoidalną podawaną z zewnątrz. Wszystkie te wyniki modelu są zgodne z charakterystykami SOAE emitowanych przez prawdziwe ucho jaszczurki.

Wnioski: Obecny model jest użytecznym rozszerzeniem wcześniejszego. Fakt, że jego charakterystyka jest odmienna niż modelu stosowanego do opisu wytwarzania SOAE przez uszy ssaków, ponownie pociąga za sobą dyskusję, czy dla różnych gatunków zwierząt potrzebne są różne modele generacji SOAE.

Słowa kluczowe: ucho wewnętrzne • oscylatory sparowane • brodawka podstawna • fala wędrująca • samopodtrzymujący • stabilizacja częstotliwości

Introduction

Otoacoustic emissions are faint sounds emitted by the ear, either spontaneously or in response to an incoming sound stimulus. They were first discovered more than 40 years ago by Kemp [1,2], confirming startling predictions made much earlier by Gold [3]. Among the several classes of otoacoustic emissions (OAEs), click-evoked and distortion product OAEs have become an integral part of clinical tests of human hearing [4].

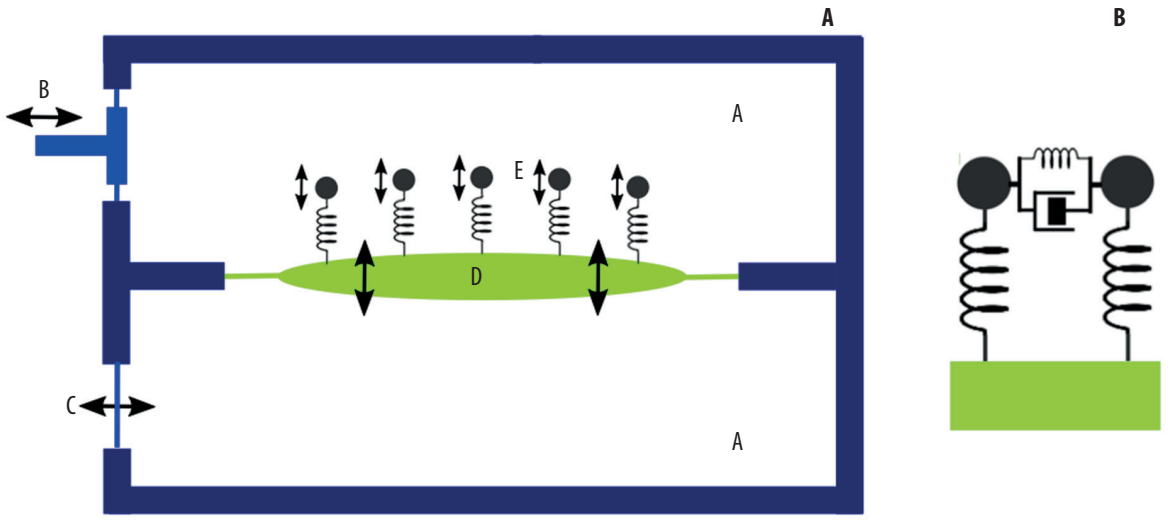

Figure 1. (**A**) Model of the inner ear of the lizard. A, fluid inside a bony cavity; B, stapes; C, round window; D, basilar papilla; E, vibrating elements (oscillators). (**B**) Detail of **A**, for the situation where the neighbouring oscillators are reactively and dissipatively coupled

A special class of OAEs are spontaneous otoacoustic emissions (SOAEs), which are tone-like sounds emitted by an ear in the absence of any acoustic stimulation. The resulting spectrum of these sounds shows one or several distinctive peaks, suggesting that perhaps the ear contains a set of fixed resonant elements, almost like a set of piano strings. Although SOAEs are not used in clinical practice, they are extensively investigated because they evidently reflect some internally active (amplification) process that improves the ear's sensitivity and selectivity. Gold [3] suggested comparing the ear, being filled with fluid, with an underwater piano in which the vibration of the strings is amplified to compensate for the heavy damping of the surrounding fluid [5]. Overcompensation would then result in the emission of pure tones, just like SOAEs might be produced.

However, despite intensive research into their behaviour, the mechanism behind SOAEs has proved elusive, and there is still controversy in the field. In attempting to resolve the issue, there has been a longstanding interest in the hearing of lizards and other reptiles [6,7] because their ears are simpler than those of mammals. At the same time, both classes of animal share a number of features, most notably the generation of SOAEs, and the general hope is that understanding the lizard ear will prove helpful in understanding human hearing.

One of the ways to gain insight into this generation process is to make a physically realistic model of the lizard ear and perform numerical computations that allow its behaviour – especially its acoustic spectrum – to be compared with experimentally obtained data. This is the approach taken in the present paper.

In the lizard ear model by Vilfan & Duke [8] and by Gelfand et al. [9], a spontaneous otoacoustic emission (SOAE) signal is regarded as the sum of the displacements (as a function of time) of coupled oscillators in a one-dimensional array. Individual peaks in an SOAE spectrum might therefore reflect the combined displacements of neighbouring oscillators clustered into frequency plateaus [10]. This same model was used by Wit and colleagues [11,12] to explain several characteristics of different types of otoacoustic emissions from lizard ears.

Not incorporated in the model, however, is how the sum of individual oscillations is transmitted to the tympanic membrane. It therefore overlooks the possibility that this transmission process might in some way change the emitted signal. A model of the lizard ear by Bergevin & Shera [13] does include coupling to the middle ear, and thereby to the external acoustic environment, but it describes only stimulus frequency otoacoustic emissions (SFOAEs). In their model, hair bundles are represented by damped harmonic oscillators, but since the oscillators are passive, the model cannot describe the generation and emission of spontaneous otoacoustic emissions. (For detailed arguments, see the thorough overview of OAE modelling by Bergevin et al. [14]).

The present work seeks to overcome this limitation by representing each of the hair bundles as an active mechanical system that can generate self-sustained oscillations at a characteristic frequency [15]. It uses the formalism applied earlier by Vilfan & Duke [8], where the parameters can be varied so as to change both the properties of the oscillators and the way they are coupled. This model was used in the earlier work of Wit et al. [12]. Here, the model is elaborated to include the middle ear so that spontaneous activity of the hair bundles can be conveyed to the eardrum.

The model

Figure 1 is a schematic drawing of the lizard ear. It is based on the following figures: Fig. 1 of [13], Fig. 3A of [16], Fig. 1 of [17], Plate 1 in [18], Fig. 1 in [19], and Fig. 3 in [20]. The basilar papilla in **Figure 1** moves as a rigid element [21,22]. It is connected to the surrounding structure by elastic elements (Fig. 6 of [19]). The vibrating elements (hair cells) set the basilar papilla into motion. This motion is transported to the stapes through the incompressible fluid and leaves the ear as an otoacoustic emission.

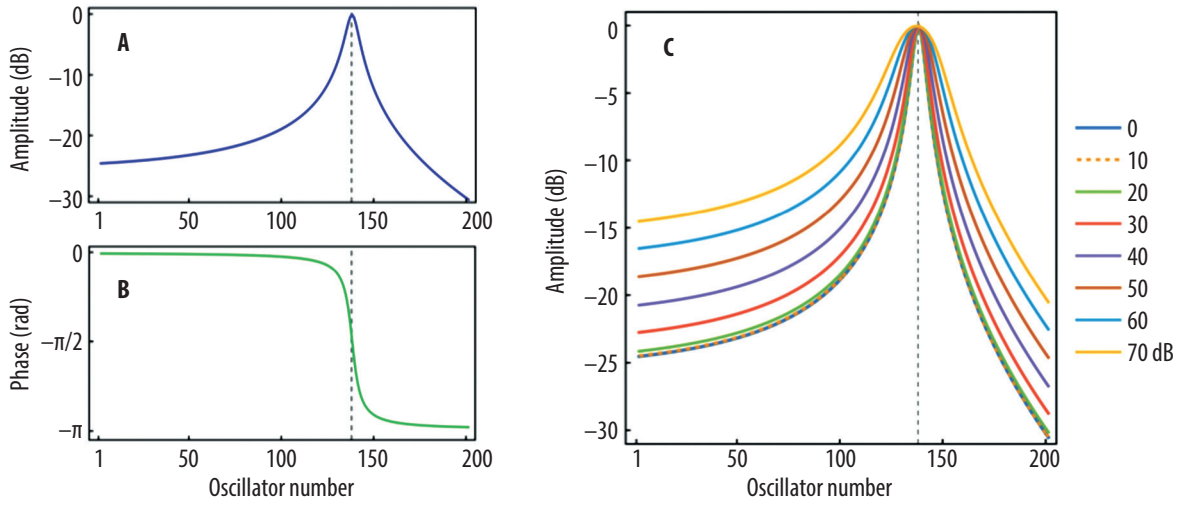

Figure 2. Amplitude and phase of the sinusoidal oscillation $x_j(t)$ of oscillators 2–201, if oscillator 1 is driven with a 3 kHz continuous sine wave with different amplitudes a. (**A**) Amplitude, for $a = 1$. (**B**) Phase with respect to that of oscillator 1, also for $a = 1$. (**C**) Amplitude for a increasing from 1 (0 dB) to 70 dB in 10 dB steps. (All curves are normalised to have maximum amplitude 1). The dashed lines in all panels mark oscillator 138, with a natural frequency of 3 kHz

Figure 1 is the simplest schematic representation of the positions of, and the connections between, the vibrating elements in the lizard inner ear. It is essentially the same as Fig. 4 of [23] or Fig. 1 of [13]. The hair cells in **Figure 1** are represented by a chain of $j = 2,3, \ldots n$ coupled oscillators [1], in which x_j and $\dot{x}_j$ are, respectively, displacement and velocity (as a function of time) of the j^{th} oscillator. If x_j and $\dot{x}_j$ are combined in the complex notation $z_j = x_j - \frac{1}{\omega_j} i x_j$, the differential equation to be solved for the j^{th} oscillator ($j = 2,3,\ldots,n$) is:

$$\dot{z_j} = (i\omega_j + \epsilon_j)z_j + (d_R + id_I)(z_{j-1} - 2z_j + z_{j+1}) - b|z_j|^2 z_j \qquad (1)$$

In Equation (1), ω_j is the natural frequency of oscillator j (the frequency with which it will oscillate if it is not coupled to its neighbours); ϵ_j is a measure of the effective damping, being positive for an active oscillator and negative for a passive (damped) oscillator; d_R and d_I are dissipative and reactive coupling constants respectively; and b_j controls the oscillation amplitude. For the first oscillator of the chain of vibrating elements ($j = 2$) the term $(z_{j-1} - 2z_j + 2z_{j+1})$ is replaced by $(z_3 - z_2)$ and for the last by $(z_{n-1} - z_n)$. Without coupling ($d_R = d_I = 0$), each oscillator obeys the generic equation for a Hopf bifurcation [24]:

$$\dot{z_j} = (i\omega_j + \epsilon_j)z_j - b|z_j|^2 z_j \,.$$

Because the fluid is incompressible, the elements A, B, C, and D in **Figure 1** move together at one frequency, and hence they are simply represented by only one damped oscillator. The displacement as a function of time, $Re[z_1(t)]$ of this oscillator is then the otoacoustic emission (OAE) measured at the eardrum. The equation for this oscillator is:

$$\dot{z_1} = (i\omega_1 + \epsilon_1)z_1 - b|z_1|^2 z_1 + \mu\sum_{j=2}^{n} Re[z_j] \,. \qquad (2)$$

The last term in Equation (2) stands for the total force exerted on the papilla by the vibrating elements. This force is supposed to be proportional to the sum of the displacements $x_j(t)$ of the vibrating elements, with proportionality constant μ. Furthermore, the term $+\mu Re[z_1]$ is added to the right-hand side of Equation (1), being the force exerted by the papilla on each vibrating element. The values for ω_1 and ε_1 were chosen to give the oscillator the natural frequency and the damping of the middle ear of the lizard, to approximate Fig. 2.5A in [25].

The set of differential equations, as given in Equations (1) and (2), was solved with Mathematica 12 procedure *NDSolve*.

Results

In the following we investigate different arrangements of mechanical coupling between the ear's vibrating elements (as depicted in **Figure 1**). The coupling is considered to be between nearest neighbours only, and to be a combination of masses, elasticities, and damping, covering all theoretical possibilities. In addition, at some points we consider the oscillators to be passive, and at other times active (that is, they have an inbuilt energy source that makes the elements oscillate continuously). For the situation where the oscillators are considered active, special attention is then focused on the vibration pattern of oscillator 1 (the underlying papilla on which all the elements sit), because this represents the SOAE emitted by the model.

Passive oscillators, with and without nearest neighbour coupling, sine wave stimulus

All vibrating elements that represent hair cells were given the same negative value for ε_j, and the equations were solved for the situation in **Figure 1** that the vibrating elements were coupled to the papilla only, and not to their neighbours. Oscillator 1 was driven by a continuous sine wave by adding the term $a\sin[\omega_{ext}t]$ to the righthand side of Equation (2). The parameters had the following values:

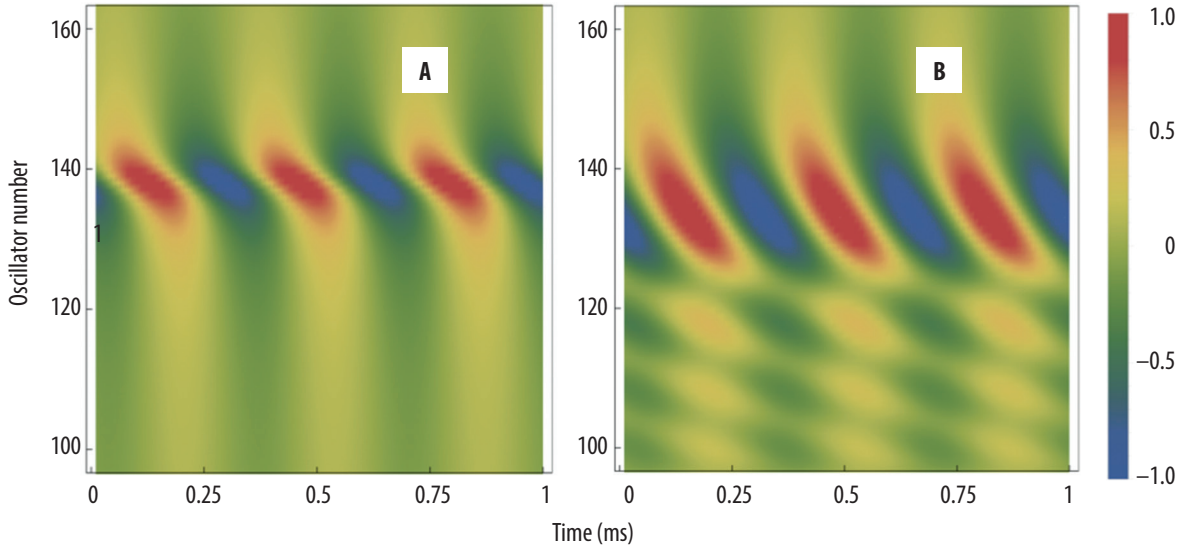

Figure 3. Density plots for the sinusoidal oscillation $x_j(t)$ for oscillators 98–162, if oscillator 1 is driven with a 3 kHz continuous sine wave. (**A**) For the same set of parameters as for Figure 2 (no nearest neighbour coupling). (**B**) For nearest neighbour reactive coupling constant $d_I = -8$, instead of 0

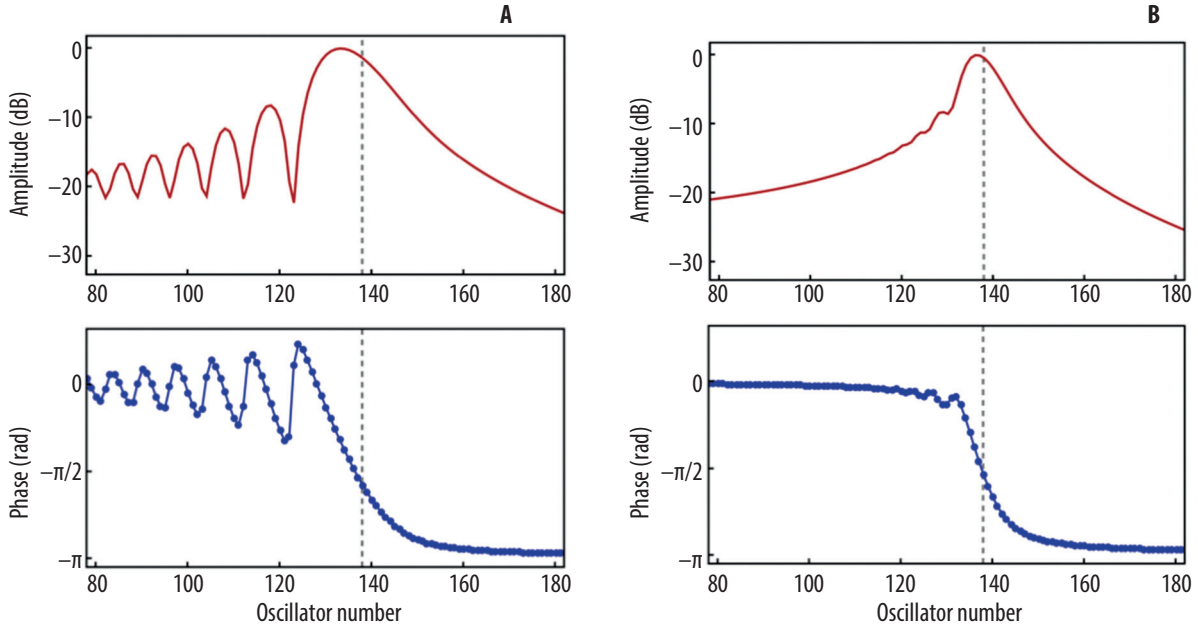

Figure 4. (**A**) Amplitude (upper panel) and phase (lower panel) of the sinusoidal oscillation $x_j(t)$ of oscillators 98–162, if oscillator 1 is driven with a 3 kHz continuous sine wave. Parameters are the same as for the calculation of Figure 2, except for the value of d_I being –8 instead of 0. The dots in the lower panel mark the phases of individual oscillators. (**B**) As for **A**, but now for $d_I = -1$. The dashed lines are at the same position as in Figure 3

$n = 201$, $\omega_1 = 2 \times 2\pi$, $\varepsilon_1 = -4$, $\varepsilon j = -0.5$, $b = 1$, $d_R = 0$, $d_I = 0$, $\mu = 0.2$, $\omega_{ext} = 3 \times 2\pi$ (being the natural frequency of oscillator 138). The natural frequencies of the oscillating elements increased exponentially from $\omega_2 = 1 \times 2\pi$ to $\omega_n = 5 \times 2\pi$. Total calculation time and time-step were 70 ms and 0.01 ms respectively. To obtain **Figure 2**, amplitude and phase were calculated for the last 50 ms of the real part of $z_j[t]$, to eliminate onset effects.

Figure 3A is a density plot for displacement as a function of time for oscillators 98 to 162, for the same set of parameters as for the calculation of **Figures 2A** and **2B**. To obtain **Figure 3B**, strong nearest neighbour coupling was introduced by changing the value of the reactive coupling constant d_I from 0 to –8. The other parameters remained the same as for **Figure 3A**. This nearest neighbour coupling has two effects, as can be seen by comparing **Figures 3A** and **3B**. First, it shifts the resonance peak – as shown in **Figure 2A** – to lower oscillator numbers and broadens it.

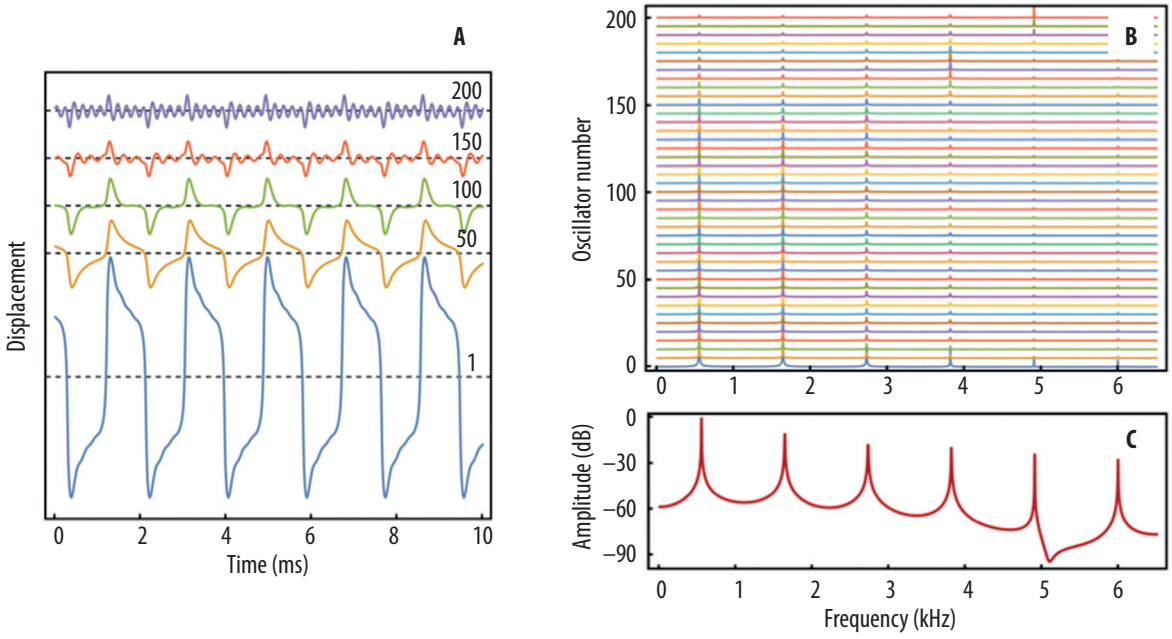

Figure 5. (**A**) Displacement as a function of time for oscillators 1, 50, 100, 150, and 200 when oscillator 1 was coupled to all of them with $\mu = 3.4$ (and no nearest neighbour coupling). Dashed lines are at displacement zero. (**B**) Amplitude spectrum with linear axes for oscillators 1, 5, 11,..., 201. (**C**) Amplitude spectrum for oscillator 1 with equidistant peaks

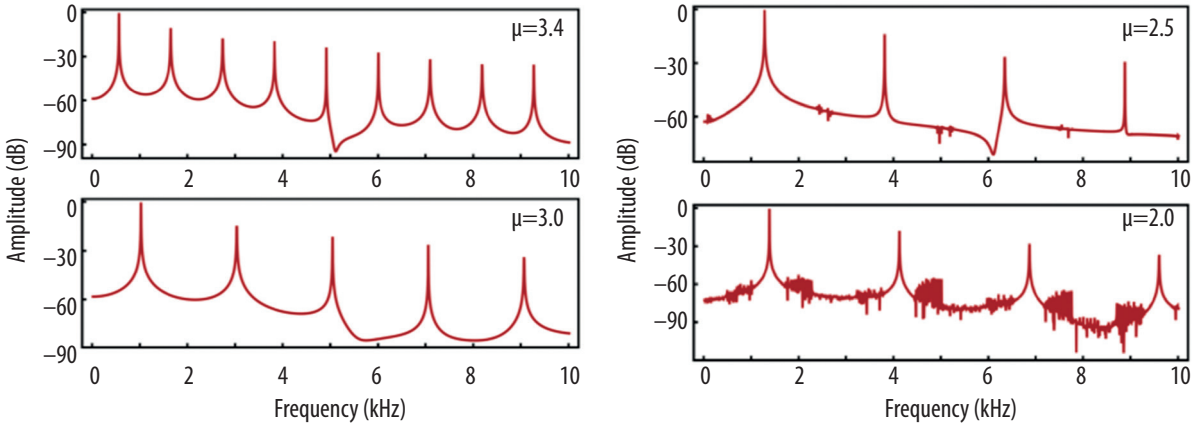

Figure 6. Amplitude spectra for oscillator 1, for decreasing values of coupling parameter μ. The irregularities in the two right panels are caused by fluctuations in the envelope of signal $x_1(t)$

And second, it creates clusters of oscillators, whose phase changes steadily along the array, with sudden phase jumps between successive clusters.

The plots in **Figure 4** show, in comparison with **Figure 2**, shifting and broadening of the resonance peak, as well as phase glides and jumps, caused by nearest neighbour coupling between the oscillators.

Active oscillators coupled to the papilla only

To couple the oscillators to the basilar papilla only (without nearest neighbour coupling), μ was given the value 3.4, with $d_R = d_I = 0$ (this was the highest value of μ for which the model remained stable). The values for ε_1 and b were 0.8. As can be seen in **Figure 5**, this produced highly distorted signals for all oscillators, with a fundamental frequency of 0.55 kHz and many odd harmonics.

Calculations were repeated for different values of μ, again for coupling to oscillator 1 only. Spectra are shown in **Figure 6**. The irregularities in the spectra for the two lower μ-values are caused by irregularities in the envelope of the signal $x_1(t)$ – that is, there are irregular fluctuations in its amplitude. For $\mu < 0.9$ the oscillators do not cluster.

Active oscillators coupled to the papilla, with nearest neighbour coupling

Amplitude spectra were calculated for the situation with nearest neighbour coupling ($d_R = 0.1$, $d_I = 1.1$), while all oscillators (vibrating elements in **Figure 1**) were coupled to

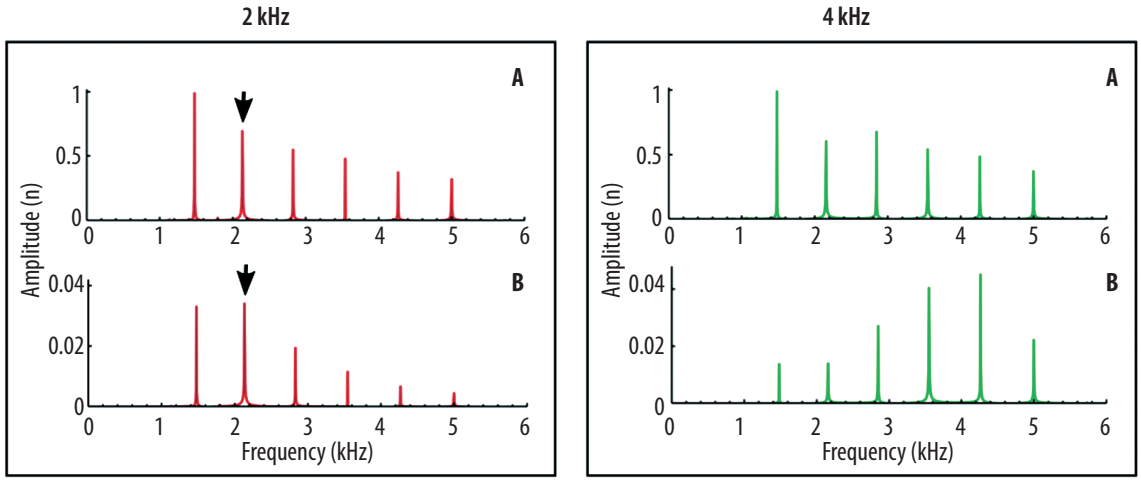

Figure 7. Amplitude spectra of oscillators for two values of basilar papilla tuning (2 and 4 kHz, left and right panels). (**A**) Amplitude spectrum for the sum of the displacements as a function of time for oscillators 2,..., 201. (**B**) Spectrum for the displacement as a function of time for oscillator 1. The arrows indicate the centre frequency of the filter that was employed to obtain Figure 8

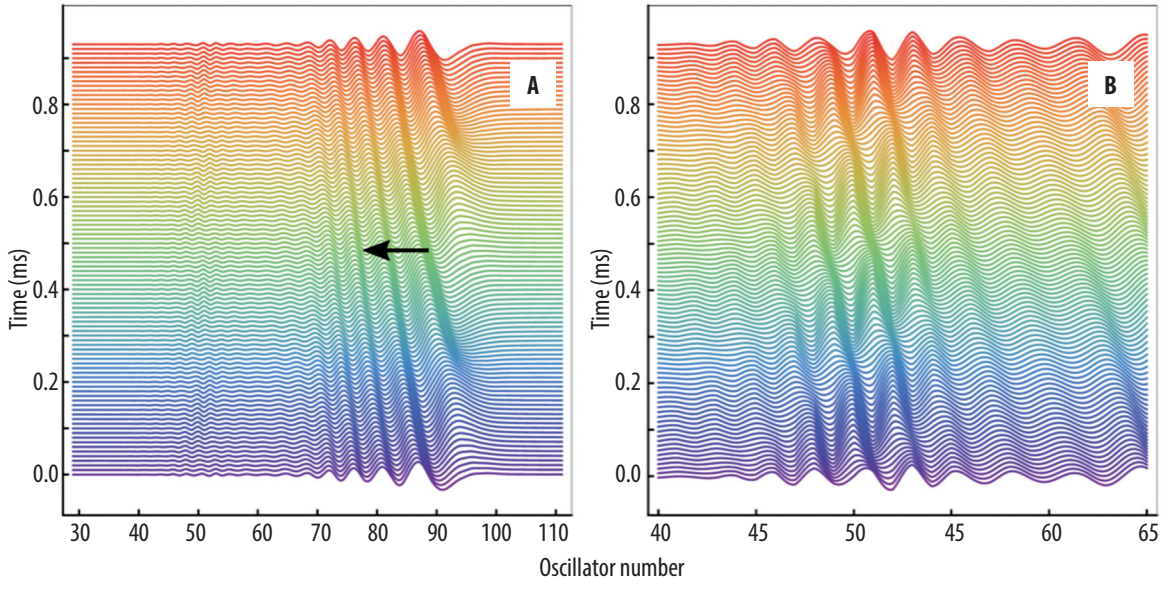

Figure 8. (**A**) Waterfall plots for two cycles of the displacement pattern of those oscillators which cluster at a frequency of 2.13 kHz. The wave-like pattern travels towards the low frequency end of the array, as indicated with the arrow. (**B**) Detail of **A**, showing a small standing-wave-like pattern

the papilla (oscillator 1; $\mu = 0.4$). The values for ε_j (2, …, 201) and for b remained at 0.8. Results are shown in **Figure 7**, for two values of the natural frequency of oscillator 1.

The two-dimensional array of $x_j(t)$ values (1, 2,..., m) was filtered with a fourth-order Butterworth filter with centre frequency 2.13 kHz and full width 200 Hz. This centre frequency (arrows in **Figure 7**) is the frequency at which a subset of the oscillators cluster. The filtered array was transposed, producing an array of displacement profiles along the oscillator array at successive times (time-step 0.01 ms). These profiles were smoothed using interpolating functions and then plotted in **Figure 8**.

Oscillators coupled to the papilla with nearest neighbour coupling, and an irregular array of ε_j values

For each ear of a lizard with SOAEs, the spectrum of the emitted sound is unique [26,27] and in general different from the regular spectra as shown in **Figure 7**. To account for this uniqueness in human ears, Fruth et al. [28] introduced, in their one-dimensional active oscillator model for the human cochlea, a different bifurcation parameter profile $\varepsilon(x)$ for each individual ear. This profile is generated by a spatial version of the stochastic Ornstein-Uhlenbeck process, producing correlation in $\varepsilon(x)$ over a finite correlation length, where x is the distance from the stapes along the

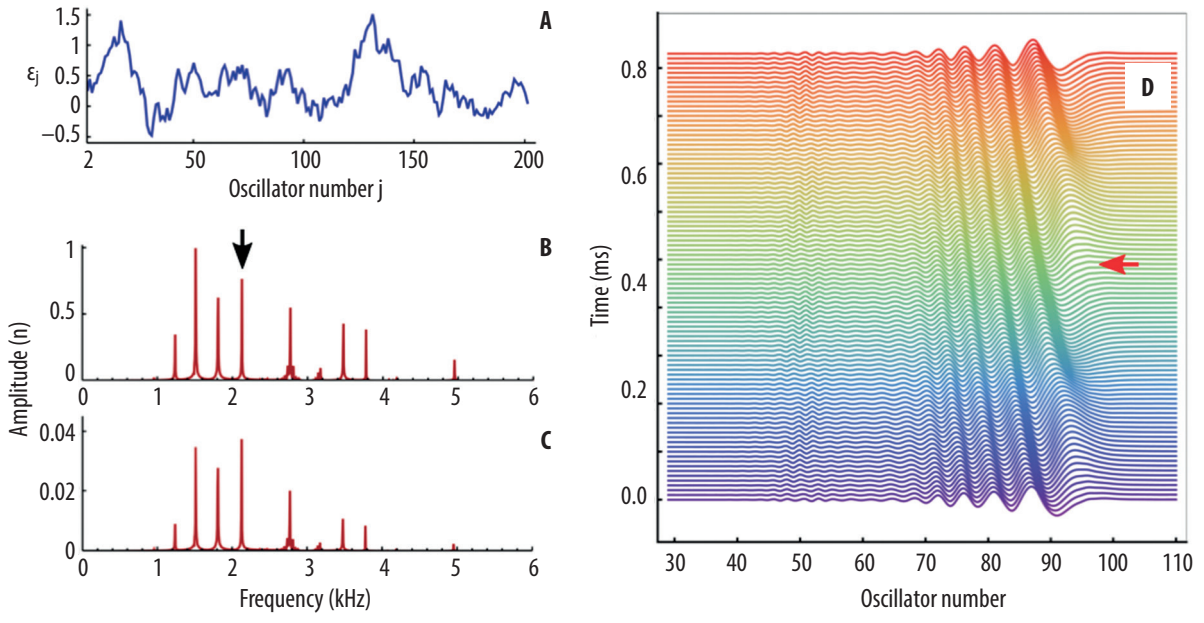

Figure 9. Response of a coupled set of oscillators with irregular $\varepsilon_j(t)$ values. (**A**) Values of ε_j for $j = 2,\ldots 201$. (**B**) Amplitude spectrum for the sum of the displacements as a function of time for oscillators 2,...201. The black arrow indicates the central frequency of the filter that was employed to obtain figure **D**. (**C**) Amplitude spectrum for the displacement as a function of time for oscillator 1, for a natural frequency of 2 kHz for this oscillator. (**D**) Waterfall plot for two cycles of the displacement pattern of those oscillators which are clustered at a frequency of 2.12 kHz. The pattern travels in the direction of the low frequency end of the array, as indicated with the red arrow

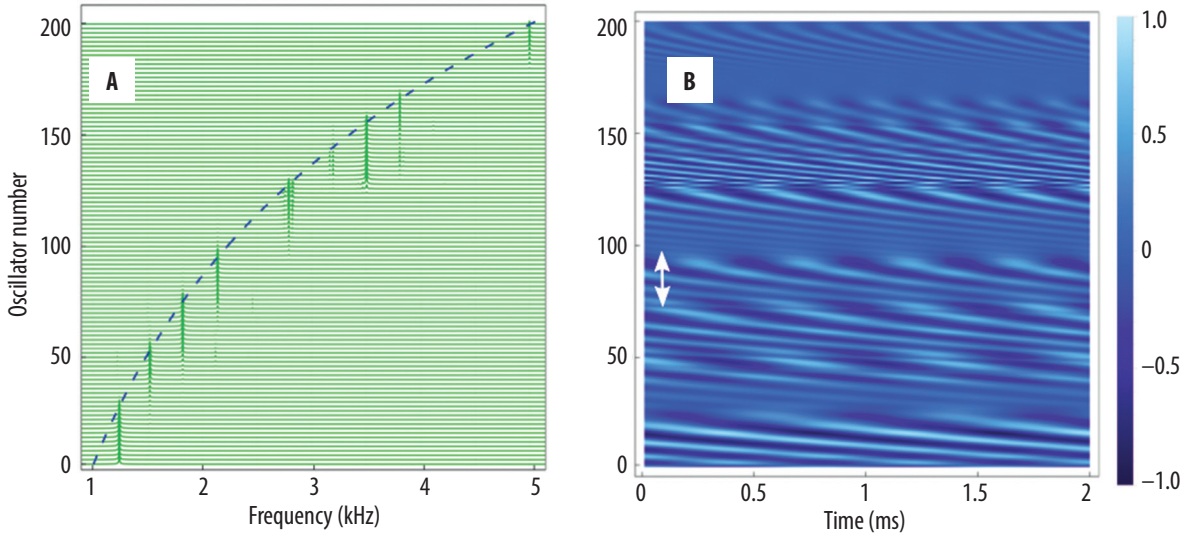

Figure 10. (**A**) Amplitude spectra for oscillators 2, 4,... 200 in a waterfall plot. Note that there are 8 distinct regions where oscillators cluster at a common frequency. The dashed line marks the natural frequencies of the oscillators. (**B**) Density plot over 2 ms for the (normalised) displacements $x_j(t)$ of oscillators 2–200. The white double-headed arrow spans the group of oscillators that cluster at 2.12 kHz

basilar membrane. According to Fruth et al. [28], correlation of irregularities along the cochlear partition could be a result of irregularities in the developmental process.

Following Fruth et al. [28], calculations were repeated for the same set of parameters as used to obtain **Figures 7** and **8** above, but now for the εj-profile shown in **Figure 9A**, instead of for a constant value of εj. This profile was calculated with Mathematica command *RandomFunction[OrnsteinUlhenbeckProcess]*. Spectra given in **Figures 9B** and **9C** should be compared with those in **Figure 7**. The moving displacement profile in **Figure 9D** was calculated in the same way as **Figure 8**, applying a bandpass Butterworth filter.

Figure 10A shows the amplitude spectra for oscillators 2, 4,… 200 in a waterfall plot. And **Figure 10B** is a density plot for the (normalised) displacements $x_j(t)$ of oscillators

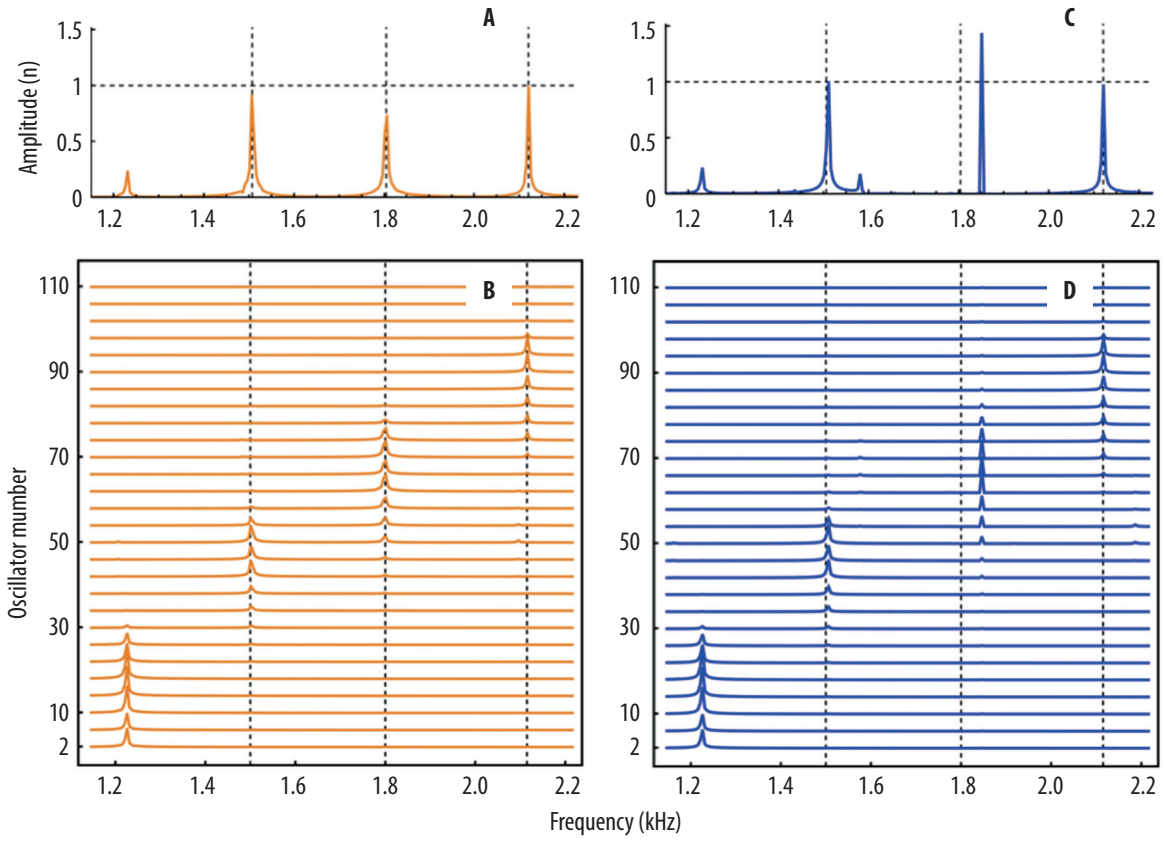

Figure 11. The oscillator system driven by an external tone of 1.85 kHz, with results plotted from 1.2 to 2.2 kHz. (**A**) Detail of the amplitude spectrum for oscillator 1, for the same set of parameters as for Figure 9. (**B**) Amplitude spectra for a subset of the individual oscillators, again for the same set of parameters as for Figure 9. (**C**) As for **A**, but now with a 1.85 kHz continuous force driving oscillator 1. (**D**) As for **B**, but with the force now present. The vertical gridlines are in the same positions in all panels

2–200 during 2 ms. The white arrow marks the range of oscillators that cluster at a frequency of 2.12 kHz, producing the spectral peak marked with a black arrow in **Figure 9B**.

Entrainment by an external tone

Amplitude spectra were again calculated for the same set of parameters as for the preceding subsection, and results are shown in **Figure 11A** (which is a detail of **Figure 9C**). These calculations were repeated after the introduction of a continuous sinusoidal force driving oscillator 1. This force was given a frequency of 1.85 kHz, being slightly higher than that of the 1.8 kHz cluster of oscillators in **Figure 11B**. Its strength was just enough to fully entrain the cluster, as can be seen by the 1.85 kHz peak and cluster in **Figures 11C** and **11D**.

Discussion

The numerical modelling undertaken here has been generally guided by experience from previous work on the dynamical properties of arrays of active oscillators. This experience has informed the choice of parameters, although it must be acknowledged that the parameter space has not been thoroughly explored. Nevertheless, some interesting properties have emerged from the present work, and the relevance to the lizard ear is discussed in more detail below, following the arrangement of the Results section.

Passive oscillators

We have seen that the sharpness of tuning, shown in **Figure 2C**, decreases for increasing amplitude *a* of the constant frequency sinusoidal force that stimulates oscillator 1. This is because the equation governing the behaviour of the oscillating elements 2–201 is that for a Hopf resonator, and for such a resonator the sharpness of tuning decreases for larger amplitudes of the sinusoidal driving force (see, for instance, Fig. 2 in [17] or Fig. 1b of [8]). This leads to the consequence that the tuning of an array of equal oscillators with a Hopf bifurcation, only differing in natural frequency, is sharper for a lower level of the stimulating constant frequency sinusoidal force, as can be seen in **Figure 2C**.

Another consequence of a Hopf-style nonlinearity has been documented for the mammalian ear by Ruggero (Fig. 1 in [29]): tuning curves, measured at one location of the basilar membrane of the chinchilla, are broader for a stronger stimulating force. The same property is seen in hair bundles of the bullfrog sacculus [30,31].

Support for the presence of a similar nonlinearity in the lizard ear comes from Holton & Weiss [32]. These authors measured receptor potential iso-voltage contours, from the same hair cell in the intact alligator lizard cochlea (their Fig. 2), for both the DC-component and for the fundamental AC-component. The narrow tip of the AC

iso-voltage contour could be recorded at sound pressure levels 20 dB lower than for the broader tip of the DC iso-voltage contour. In other words, tuning is sharper for lower stimulus levels.

The physical arrangement of the lizard ear, given in **Figure 1**, resembles that of the familiar vibrating reed frequency meter (VRFM). The only difference is that in the lizard ear the basilar papilla is attached to the surrounding cartilage-like ring by a flexible structure, while in the VRFM the individual oscillators (the "reeds") are attached to a solid bar. The VRFM was used by Wilson [33,34] to investigate the properties of the travelling wave. It was also used by von Békésy (Chapter 12 in [35]), to understand how a travelling wave arises on the mammalian basilar membrane. To couple the reeds Wilson intertwined a rubber thread between them. His findings and other properties of the VRFM are extensively treated in Bell & Wit [36].

In both the VRFM and the present model, the vibrating elements are coupled to a solid structure. So it is not surprising that the results for the situation where the oscillators in the present model are passive are identical to those for the "reeds" in [36]. In fact, **Figures 3** and **4** above are essentially the same as the respective Fig. 4 and 10c in [36].

The magnitude and spacing of the ripples, as seen in **Figure 4**, depend on the coupling strength. Stronger coupling increases both their magnitude and spacing, as can be seen in Fig. 10 of [36].

Active oscillators coupled to the papilla only

In this situation (see **Figure 5**) the waveforms of the displacements μ of all oscillators are highly distorted, giving spectra for all oscillators with the same fundamental frequency and the same harmonics. The fundamental frequency, and thus the interval between harmonics, is smaller for stronger coupling to the papillla (**Figure 6**). Considering the characteristics of SOAEs emitted by a real lizard ear (e.g. [26]), these results suggest that it is very unlikely that lizard SOAEs are created by oscillating elements that are coupled only to the papilla.

Active oscillators coupled to the papilla, with nearest neighbour coupling

The spectra in **Figure 7** have a regular pattern, although the spectral peaks are not perfectly equidistant. The peaks occur at 1.48, 2.13, 2.83, 3.54, 4.26, and 5.00 kHz (with separations of 0.65, 0.71, 0.72, and 0.74 kHz). Peak height is affected by the natural frequency of oscillator 1, an effect which is largest in the spectra for oscillator 1 (the lower panels in **Figure 7**).

Changing the resonance frequency of the highly damped oscillator 1 from 2 kHz to 4 kHz affects the amplitudes of the spectral peaks in **Figure 7**, not only for oscillator 1 but also for the sum of displacements. It does not, however, change the frequency of the peaks. It is already known that the position of the peaks and their separation depends on their reactive coupling (see Figs 5, 6, and 17 of [12]), with frequency shifts being proportional to the coupling strength parameter d_I.

The peak in the lower figure (for oscillator 1) in the left panel of **Figure 7**, marked with the arrow, is 21 times (26 dB) weaker than that for the sum of signals (upper figure in the same panel). It is impossible to check if such a difference is realistic, because the power produced by individual self-sustaining oscillators in the lizard inner ear has never been measured.

If it is supposed that the oscillator array lies in a straight row on top of the papilla, their instantaneous displacements give rise to a graded profile along the one-dimensional array. The profile travels along the array and the process repeats itself for every period of oscillation of the individual oscillators in the same cluster, as shown in **Figure 8A** for the 2.13 kHz cluster. Other clusters behave in the same way (even for other parameter settings), as can be concluded from **Figure 10**.

Although difficult to see in **Figure 8A**, but apparent in **Figure 8B**, the displacement profile for a small number of oscillators changes from a travelling wave into a low-amplitude standing wave at the transition to the 1.48 kHz cluster.

Irregular array of ε_j values

Whether the ε_j values of all oscillators are the same or irregular, the outcomes are the same: the oscillators cluster in groups of common frequency. The difference is that the spectra (**Figures 9B** and **9C**) are irregular, as are the SOAE spectra from real lizard ears [26,27]. In this context, Wit and colleagues showed (Fig. 10 in [12]) that different ε_j profiles give different spectra, in a similar way to how each individual lizard ear has its own unique SOAE spectrum.

As can be seen in **Figure 9D**, the displacement profile for the oscillators in a cluster travels towards the low frequency end of the array, and this process repeats itself after each period of oscillation.

The dashed line in **Figure 10A** indicates that the oscillators within a single cluster oscillate at the frequency of the oscillator within that cluster that has the highest natural frequency. In explanation, Vilfan & Duke [8] showed that a reactively coupled oscillator can couple only to a neighbouring oscillator that has a higher natural frequency, and never to one with a lower natural frequency.

Figure 10B illustrates how, within a cluster of oscillators, a fixed phase difference exists between adjacent oscillators. Moreover, this phase difference increases for oscillators further away from the highest frequency oscillator in that cluster (as can also be seen in Fig. 2 in [11]). After onset, the oscillators need some time to reach the stable situation shown in **Figure 10B**. This is also well illustrated in Fig. 3a of [9]: clustering starts at the high frequency end of the array and propagates towards the low frequency end. The model by Gelfand et al. [9] consists of a one-dimensional array of 110 Van der Pol oscillators, coupled to their nearest neighbours. These authors did not investigate the effect of coupling of the oscillators to the basilar papilla.

Entrainment by an external tone

If the papilla (oscillator 1) is driven by a continuous sinusoidal force, with a frequency not too far away from that of one of the clusters in the array, the oscillators in that cluster (and some in adjacent clusters) will be entrained by, and become phase-locked to, the external force (**Figure 11**). Entrainment by a sinusoidal force was demonstrated for spontaneous oscillations of hair bundles in the bullfrog sacculus [30]. For SOAEs it has been documented for humans [37] as well as for lizards [38].

Entrainment is a characteristic feature of oscillators [39]. In a model for the generation of human SOAEs, taken to be an array of coupled self-sustained oscillators, Wit & Van Dijk [40] showed entrainment of a subgroup of oscillators, clustered at one frequency, to an external sinusoidal force. If the forcing is not quite strong enough to cause permanent phase-locking – which can happen in the presence of noise – the oscillator will occasionally escape from phase-lock. This "phase-slip" is a distinctive property of (human) SOAEs, as was shown by Van Dijk & Wit [41]. The same phenomenon can also be observed in *in vitro* preparations of hair bundles of selected auditory and vestibular organs [42]. Phase-slip was modelled by Wit & Bell [43] for an array of oscillators clustered in frequency plateaus.

The phenomenon of phase-lock, and especially that of phase-slip, gives strong support for the notion that spontaneous otoacoustic emissions are generated by self-sustaining oscillators.

Concluding remarks

The model

It is generally accepted that hair cells (or their bundles) are the oscillators in a real ear. Recently, Faber & Bozovic [44] explored synchronisation of coupled hair cells in *in vitro* preparations of the bullfrog sacculus, to lend "support to the theory that SOAEs may be generated by frequency clustering of actively oscillating hair bundles". This supposition, in combination with the results and their discussion presented in the preceding sections (and the results presented in the earlier paper of Wit et al. [12]), lead to the conclusion that the basic properties of SOAEs, measurable at the lizard eardrum, can be well modelled by an array of active oscillators that are coupled to their neighbours and to the supporting papilla, as shown in **Figure 1** [23].

A dichotomy?

In Shera's wave-based "coherent reflection" model for the generation of SOAEs in the mammalian ear [45], a key role is played by standing waves created by multiple internal reflection of waves travelling backwards and forwards along the basilar membrane (Fig. 2 in [46,47]). In the present model, SOAEs are oscillators – clustered in frequency plateaus – that drive the basilar papilla of the lizard. Apart from almost imperceptible regions of the oscillator array (see **Figure 11B**), no standing waves are present. The general pattern is that of waves travelling along the array in the direction of lower natural frequencies (**Figures 7A**, **11A**, and **12D**). This observation suggests that different models are needed to describe SOAE-generation in different classes of vertebrate ears. (For a review that, among other things, addresses this question, see [14]). Bergevin and colleagues [14] think that wave-based (coherent reflection) and coupled-oscillator models "are not orthogonal notions". However, Shera argues that these two frameworks "espouse radically opposing views of causality" [48]. Adding to the discussion, Siegel recently stated that "models of otoacoustic emissions appear to be largely in error and should be reevaluated. In particular, a new generation of models that explore the direct coupling from the organ of Corti to the stapes footplate through fluid pressure appear to be required" [49]. It seems we are nowhere near the last word on this subject.

Acknowledgements

We thank Geoffrey Manley for sharing his invaluable knowledge of the lizard ear, and in particular the characteristics of its otoacoustic emissions.

References

1. Kemp DT. Active resonance systems in audition. 13th International Congress of Audiology, 1976, Abstracts 64–65.
2. Kemp DT. Stimulated acoustic emissions from within the human auditory system. J Acoust Soc Am, 1978; 64: 1386–91.
3. Gold T. Hearing II. The physical basis of the action of the cochlea. Proc Roy Soc B, 1948; 135: 492–8.
4. Probst R, Lonsbury-Martin BL, Martin GK. A review of otoacoustic emissions. J Acoust Soc Am,1991; 89: 2027–67.
5. Bell JA. The underwater piano: a resonance theory of cochlear mechanics. PhD thesis, Australian National University, 2005. https://openresearch-repository.anu.edu.au/bitstream/1885/49307/6/02whole.pdf.
6. Manley GA. Diversity in hearing-organ structure and the characteristics of spontaneous otoacoustic emissions in lizards. In: Lewis ER, Long GR, Lyon RF, Narins PM, Steele CR, editors. Diversity in Auditory Mechanics. Singapore: World Scientific; 1997, p.32–8.
7. Manley GA. Otoacoustic emissions in non-mammals. Audiol Res, 2022; 12: 260–72.
8. Vilfan A, Duke T. Frequency clustering in spontaneous otoacoustic emissions from a lizard's ear. Biophys J, 2008; 95: 4622–30.
9. Gelfand M, Piro O, Magnasco MO, Hudspeth AJ. Interactions between hair cells shape spontaneous otoacoustic emissions in a model of the Tokay Gecko's cochlea. PLoS One, 2010; 5(6): e11116.
10. Ermentrout GB, Kopell N. Frequency plateaus in a chain of weakly coupled oscillators. SIAM J Math An, 1984; 15: 215–37.
11. Wit HP, Van Dijk P, Manley GA. A model for the relation between stimulus frequency and spontaneous otoacoustic emissions in lizard papillae. J Acoust Soc Am, 2012; 132: 3273–9.
12. Wit HP, Manley GA, Van Dijk P. Modelling the characteristics of spontaneous otoacoustic emissions in lizards. Hear Res, 2020; 385: 107840.
13. Bergevin C, Shera CA. Coherent reflection without traveling waves: on the origin of long-latency otoacoustic emissions in lizards. J Acoust Soc Am, 2010; 127: 2398–409.

14. Bergevin C, Verhulst S, Van Dijk P. Remote sensing the cochlea: otoacoustics. In: Manley GA, Gummer AW, Popper AN, Fay RR, editors. Understanding the Cochlea. Springer Handbook of Auditory Research, vol 62, pp. 287–318. New York: Springer; 2017.
15. Camalet S, Duke T, Jülicher F, Prost J. Auditory sensitivity by self-tuned critical oscillations of hair cells. Proc Natl Acad Sci USA, 2000; 97(7): 3183–8.
16. Mulroy MJ. Cochlear anatomy of the alligator lizard. Brain Behav Evol, 1974; 10: 69–87.
17. Rosowski JJ, Peake WT, Lynch TJ, et al. A model for signal transmission in an ear having hair cells with free-standing stereocilia. II. Macromechanical stage. Hear Res, 1985; 20: 139–55.
18. Freeman DM. Anatomical model of the cochlea of the alligator lizard. Hear Res, 1990; 49: 29–37.
19. Aranyosi AJ, Freeman DM. Two modes of motion of the alligator lizard cochlea: measurement and model predictions. J Acoust Soc Am, 2005; 118: 1585–92.
20. Negandhi J, Bergevin C, Harrison RV. Scanning electron microscopy of the basilar papilla of the lizard (*Anolis carolinensis*). Canadian Acoustics/Acoustique canadienne, 2018; 46: 7–12.
21. Manley GA, Yates, GK, Köppl C. Auditory peripheral tuning; evidence for a simple resonance phenomenon in the lizard *Tiliqua*. Hear Res, 1988; 33: 181–90.
22. Peake WT, Ling A. Basilar-membrane motion in the alligator lizard: its relation to tonotopic organization and frequency selectivity. J Acoust Soc Am, 1980; 67: 1736–45.
23. Bergevin C. Introducing global coupling to nearest-neighbor models of SOAE generation. PS 867 in ARO Abstracts (2016) 39, 538. http://www.yorku.ca/cberge/images/2016AROsoaesPoster.pdf.
24. Eguiluz VM, Ospeck M, Choe Y, et al. Essential nonlinearities in hearing. Phys Rev Lett, 2000: 84(22): 5232–5.
25. Saunders JC, Duncan RK, Doan DE, Werner YL. The middle ear of reptiles and birds. In: Dooling RJ, Fay RR, Popper AN, editors. Comparative Hearing: Birds and Reptiles. Springer Handbook of Auditory Research, vol 13. New York, Springer; 2000.
26. Köppl C, Manley GA. Spontaneous otoacoustic emissions in the bobtail lizard. I: General characteristics. Hear Res, 1993; 71: 157–69.
27. Manley GA, Gallo L, Köppl C. Spontaneous otoacoustic emissions in two gecko species, *Gekko gecko* and *Eublepharis macularius*. J Acoust Soc Am, 1996; 99: 1588–603.
28. Fruth F, Jülicher F, Lindner B. An active oscillator model describes the statistics of spontaneous otoacoustic emissions. Biophys J, 2014; 107: 815–24.
29. Ruggero MA. Responses to sound of the basilar membrane of the mammalian cochlea. Curr Opin Neurobiol, 1992; 2(4): 449–56.
30. Martin P, Hudspeth AJ. Compressive nonlinearity in the hair bundle's active response to mechanical stimulation. Proc Natl Acad Sci USA, 2001; 98: 14386–91.
31. Ospeck M, Eguiluz VM, Magnasco MO. Evidence of a Hopf bifurcation in frog hair cells. Biophys J, 2001; 80: 2597–607.
32. Holton T, Weiss TF. Frequency selectivity of hair cells and nerve fibers in the alligator lizard cochlea. J Physiol, 1983; 345: 241–60.
33. Wilson JP. A mechanical model of travelling waves (A). Brit J Audiol, 1983; 17: 119–20.
34. Wilson JP. Cochlear mechanics. Adv Biosci, 1992; 83: 71–84.
35. Von Békésy G. Experiments in hearing. New York: McGraw-Hill; 1960.
36. Bell A, Wit HP. The vibrating reed frequency meter: digital investigation of an early cochlear model. Peer J, 2015; 3: e1333.
37. Long GR, Tubis A, Jones KL. Modelling synchronization and suppression of spontaneous otoacoustic emissions using Van der Pol oscillators: effects of aspirin administration. J Acoust Soc Am, 1991; 89: 1201–12.
38. Köppl C, Manley GA. Spontaneous otoacoustic emissions in the bobtail lizard. II: Interactions with external tones. Hear Res, 1994; 71: 157–69.
39. Pikovski A, Rosenblum M, Kurths J. Synchronization: A universal concept in nonlinear sciences. Cambridge UK: Cambridge University Press; 2003.
40. Wit HP, Van Dijk P. Are human spontaneous otoacoustic emissions generated by a chain of coupled nonlinear oscillators? J Acoust Soc Am, 2012; 132: 918–26.
41. Van Dijk P, Wit HP. Synchronization of spontaneous otoacoustic emissions to a 2f1–f2 distortion product. J Acoust Soc Am, 1990; 88: 850–56.
42. Roongthumskul Y, Shlomovitz R, Bruinsma R, Bozovic D. Phase slips in oscillatory hair bundles. Phys Rev Lett, 2013; 110: 148103.
43. Wit HP, Bell A. Clusters in a chain of coupled oscillators behave like a single oscillator: relevance to spontaneous otoacoustic emissions from human ears. J Hear Sci, 2017; 7(1): 19–26.
44. Faber J, Bozovic D. Chimera states and frequency clustering in systems of coupled inner-ear hair cells. Chaos, 2012; 31: 073142.
45. Shera CA. Mammalian spontaneous otoacoustic emissions are amplitude-stabilized cochlear standing waves. J Acoust Soc Am, 2003; 114: 244–62.
46. Shera CA, Cooper NP. Basilar-membrane interference patterns from multiple internal reflection of cochlear traveling waves. J Acoust Soc Am, 2013; 133: 2224–39.
47. Shera CA. Iterated intracochlear reflection shapes the envelopes of basilar-membrane click responses. J Acoust Soc Am, 2015; 138: 3717–22.
48. Shera CA. Whistling while it works: spontaneous otoacoustic emissions and the cochlear amplifier. JARO, 2022; 17–25.
49. Siegel J. Wide bandwidth of ear-canal otoacoustic emission signals supports fast reverse propagation from organ of Corti through fluid pressure. Abstracts 45th Annual Midwinter Meeting of the Association for Research in Otolaryngology, 2022: 128–9.